## Title

# Effects of myopia and glaucoma in the prelaminar neural canal and anterior lamina cribrosa using 1060-nm swept-source optical coherence tomography

## Running head

Myopia and glaucoma effects in anterior lamina cribrosa using SS-OCT

## Authors

Sieun Lee[1,2]; Morgan Heisler[1]; Dhanashree Ratra[3]; Vineet Ratra[3], Paul J Mackenzie[4]; Marinko V Sarunic[1]; and Mirza Faisal Beg[1]

1. School of Engineering Science, Simon Fraser University, 8888 University Dr, Burnaby BC V5A 1S6, Canada

2. Mental Health & Clinical Neurosciences, School of Medicine, University of Nottingham, Nottingham, NG7 2UH

3. Sankara Nethralaya, No. 41 (old 18), College Road, Chennai - 600 006, Tamil Nadu, India

4. Department of Ophthalmology & Visual Sciences, Faculty of Medicine, University of British Columbia, 2550 Willow Street, Vancouver, BC Canada V5Z 3N9

## Corresponding author

Sieun Lee
University of Nottingham
Beacon Hub Offices, A floor
Medical School, QMC
Nottingham, NG7 2UH
Phone: +44 078 3839 2625
Email: sieun.lee@nottingham.ac.uk

## Abstract

Purpose: Investigate the effects of myopia and glaucoma in the prelaminar neural canal and anterior lamina cribrosa using 1060-nm swept-source optical coherence tomography

Design: Retrospective, cross-sectional study

Methods:

- Setting: Clinical practice

- Patient or study population: 19 controls (38 eyes); 38 glaucomatous subjects (63 eyes). Inclusion criteria for glaucomatous subjects: i) optic disc neural rim loss; ii) peripapillary nerve fibre layer (NFL) loss on spectral domain optical coherence tomography (SD-OCT); iii) glaucomatous visual field defect with an abnormal pattern standard deviation (P<.05); iv) stable SD-OCT, visual field, and optic disc clinical examination for 6 or more months. Inclusion criteria for control subjects: no evidence of retinal or optic nerve pathology. Exclusion criteria: i) retinal diseases or optic neuropathy other than primary open-angle glaucoma; ii) intraocular pressure less than 10 mmHg or higher than 20 mmHg; iii) ocular media opacities; iv) any surgery-related complication deemed inappropriate for the study.

- Intervention or observation procedures: Swept-source optical coherence tomography

- Main Outcome Measure(s): Bruchs membrane opening (BMO) and anterior laminar insertion (ALI) dimension, prelaminar neural canal dimension, anterior lamina cribrosa surface (ALCS) depth

Results: Glaucomatous eyes had more bowed and nasally rotated BMO and ALI, more horizontally skewed prelaminar neural canal, and deeper ALCS than the control eyes. Increased axial length was associated with a wider, longer, and more horizontally skewed neural canal, and decrease in the ALCS depth and curvature.

Conclusion: Our findings suggest that glaucomatous posterior bowing or cupping of lamina cribrosa can be significantly confounded by the myopic expansion of the neural canal. This may be related to higher glaucoma risk associated with myopia from decreased compliance and increased susceptibility to IOP-related damage of LC being pulled taut.

## Introduction

Glaucoma is a leading cause of blindness in the world and a multi-factorial group of diseases involving progressive damage to the retinal ganglion cells (RGCs) and axons resulting in irrevocable vision loss. Although the etiology and mechanism of glaucoma are not yet fully understood, elevated intraocular pressure (IOP) is an important risk factor and treatment target. In experimental and clinical studies,[1–3] lamina cribrosa (LC) in the optic nerve head (ONH) has been shown as the main site of RGC axonal damage in early glaucoma, and the IOP-related deformation, remodeling, and mechanical failure of the ONH connective tissues are proposed as the defining pathophysiology of the disease.[4–6] These alterations include posterior laminar deformation,[7,8] scleral canal expansion,[8,9] posterior migration of anterior laminar insertion (ALI),[10,11] laminar thickness change,[7,12] and posterior bowing of the peripapillary sclera.[2] The biomechanical paradigm suggests that the response of an individual ONH to a given level of IOP depends on its structural factors, affecting the disease susceptibility, occurrence, and progression.

In myopia, the eye elongates in the anterior – posterior (axial) direction, causing poor focus in distance vision. The myopic elongation, particularly in high myopia, affects the ONH structure.[13–17] In the standard glaucoma examination of the ONH and peripapillary region using ophthalmoscopy and optical coherence tomography (OCT), myopia can confound the assessment with shallow cupping, pallor in the neuroretinal rim, and retinal nerve fiber layer thinning.[18–20] Furthermore, high myopia has been associated with increased susceptibility to glaucoma in several population-based studies.[21–23]

These findings suggest that myopic deformation of the ONH structure may affect the biomechanism of glaucoma development and progression.

OCT has now become a standard technology in ophthalmic clinics, providing high resolution and cross-sectional 3D images of the retina. Compared to a conventional spectral domain OCT, a swept-source OCT (SS-OCT) with a 1060-nm wavelength source allows for visualization of deeper structures in the ONH. Using SS-OCT, we have previously published on the morphological characteristics of the ONH and peripapillary region in myopic normal and glaucomatous subjects.[24–26] We showed that axial length was a significant factor in the shape of Bruch's membrane opening (BMO) and the degree of posterior bowing of the peripapillary BM. In the present study, we extend the investigation to the prelaminar neural canal between BMO and ALI and anterior lamina cribrosa morphology in healthy and glaucomatous myopic subjects to further examine the structural effects of myopia and glaucoma in the ONH.

# Materials and Methods

## Participants

The study was conducted in accordance with the Declaration of Helsinki and approved by the institutional research ethics boards of Simon Fraser University (SFU) and University of British Columbia (UBC). Myopic participants with and without glaucoma were included following a full clinical examination by a fellowship-trained glaucoma specialist (PJM), including dilated stereoscopic imaging, IOP measurement using Goldmann applanation tonometer, and reproducible Humphrey SITA-Standard white-

on-white visual field. Axial length was measured using Zeiss IOLMaster (Carl Zeiss Meditec, Jena, Germany).

The glaucomatous eyes included in the study met the following criteria: i) evidence of optic disc neural rim loss on clinical examination; ii) evidence of peripapillary NFL loss on spectral domain optical coherence tomography (SD-OCT); iii) glaucomatous visual field defect with an abnormal pattern standard deviation (P<.05); iv) stable SD-OCT, visual field, and optic disc clinical examination for 6 or more months. The nonglaucomatous eyes included in the study showed no evidence of retinal or optic nerve pathology. From both groups, eyes were excluded based on following criteria: i) retinal diseases or optic neuropathy other than primary open-angle glaucoma, including myopic degeneration; ii) IOP lower than 10 mmHg or greater than 20 mmHg; iii) ocular media opacities; iv) any surgery-related complication that the investigators determined inappropriate for the study.

## Image acquisition and processing

The participants were imaged at the Eye Care Centre, Vancouver General Hospital, using a custom swept-source optical coherence tomography (SS-OCT) system with a 1060-nm light source, built by Biomedical Optics Research Group at SFU. The system had 100 KHz A-scan rate and 1.6 second imaging time with improved visualization of deeper ONH structures compared to conventional 800-nm range commercial OCT systems. The acquired volumetric images consisted of 400 B-scans with voxel dimension of 1024 x 400. The axial resolution was 2.8 µm and the lateral resolution was 11 to 20 µm, depending on the axial length of the eye. Axial motion correction and bounded variance smoothing was applied to improve the image quality.

## Segmentation

Bruch's membrane (BM), Bruch's membrane opening (BMO), anterior laminar insertion (ALI), and anterior lamina cribrosa surface (ALCS) were segmented (Figure 1-A). BM was segmented automatically using a 3D graph-cut based method[25] and the result was examined and corrected for segmentation errors by trained raters. BMO, ALI, and ALCS were segmented manually using Amira (Thermo Fisher Scientific, MA) on 80 radial slices extracted from the OCT volume, intersecting at the approximate centre of BMO and equidistanced at 2.25°.

## Shape Parameterization

The prelaminar region was approximated as an oblique cylinder, open at the top by BMO, and closed at the bottom by ALCS outlined by ALI. Parameters were defined to characterize the geometry of the cylinder and grouped into BMO and ALI parameters, prelaminar neural canal parameters, and ALCS parameters. BM plane was used as the reference, computed by principal component analysis (PCA) on BM points at 2 mm away from BMO.

### BMO and ALI

BMO and ALI were modelled as ellipses and measured for their sizes, lateral elongation, axial nonplanarity, and distance from BM (Figure 1-B). For geometrical analysis of BMO, an ellipse was fitted to the 160 segmented BMO points by computing the best-fit plane using PCA and fitting an ellipse to the projection of the points on the plane using the minimum squared error criterion. The area, location of the centroid, and major and minor axes were obtained from the BMO ellipse. BMO lateral elongation was characterized by eccentricity (ratio of the major and minor axes) and direction in the

enface plane (angle between the BMO ellipse major axis and superior-inferior axis). BMO nonplanarity was calculated as the mean normal distance of the segmented BMO points to its own best-fit plane. This was also normalized to relative nonplanarity by dividing BMO nonplanarity by BMO area. BMO distance from BM was measured as the normal distance between the BM plane and BMO centroid. Same parameters were computed for ALI. The ellipse fitting approach mitigates the effects of heavy blood vessel shadowing in the ONH region and resulting difficulty of segmenting BMO or ALI points in some slices.

### Prelaminar Neural Canal

Prelaminar neural canal was measured for the dimension (length, height, width) and direction (axial and lateral angles), and the difference between the anterior and posterior ends (expansion, bowing, twist) as follows (Figure 1-C). First, canal axis was defined as the vector between the BMO centroid and ALIP centroid. Canal length was defined as the length of the vector, and the height and width as the lengths of the axial and lateral components of the vector. Canal angle was measured as the angle between the canal axis and the vertical (axial) axis of the image, and the enface canal direction was measured as the angle between the lateral component of the canal axis and the superior-inferior axis. The differences between the BMO and ALIP areas (posterior expansion), eccentricities, nonplanarity, and major axes (twist) were also measured.

### ALCS

ALCS was measured for the degree of surface cupping (depth, curvature), and off-centeredness of the deepest point (Figure 1-D). The parameters were measured for the

manual ALCS segmentation points and their least square-fit quadratic polynomial surface.

Mean ALCS depths were computed as the average normal distances from the ALI plane to the segmented points and to the fitted surface on a 0.01 mm grid. The mean depth was also normalized by dividing by the ALI area. For the fitted surface, mean curvature and the relative enface position of the ALCS minimum (defined as the deepest point on the surface) to the ALI centroid were measured.

### Statistical Analysis

The nonglaucomatous and glaucomatous groups were compared using generalized estimation equation analysis, accounting for the inter-eye correlation and including age and axial length in the model to adjust for any confounding. The effects of age and axial length in the nonglaucomatous group and the effects of age, axial length, and visual field mean deviation (MD) in the glaucomatous group on the shape parameters were evaluated using a mixed effect model with a random subject effect for the inter-eye correlation. SPSS 24 (IBM Corp. Released 2016. IBM, Armonk, NY) and SAS (SAS Institute Inc., Cary, NC) were used for the analysis.

## Results

The characteristics of the study population are listed in Table 1. There was a significant difference in the age and visual field mean deviation (MD) between the nonglaucomatous and glaucomatous groups.

The mean results for Bruch's membrane opening (BMO), anterior laminar insertion (ALI), prelaminar neural canal (PNC) and anterior lamina cribrosa surface (ALCS) for nonglaucomatous and glaucomatous eyes are shown in Table 2.

Significant p-values (< .05) from the general linear models of the measurements with age and axial length (AL) as predictors for nonglaucomatous eyes and with age, AL, and visual field index (MD) are shown in Table 3.

## Bruch's Membrane Opening and Anterior Laminar Insertion

BMO **area** and **eccentricity** were not significantly different between the nonglaucomatous and glaucomatous eyes (Table 2) but longer axial length was associated with a larger and more elliptical BMO was associated in both groups (Table 3). Compared to BMO, ALI area was larger and similarly associated with longer axial length in both nonglaucomatous and glaucomatous eyes (Table 3).

BMO and ALI **nonplanarity** is visualized for a representative eye in Figure 2. On the right side, the normal distance of the BMO and ALI points are plotted in reference to their own best-fit planes, starting from the temporal axis and progressing in the clockwise direction. The plot shows BMO and ALI shape in the axial direction, with nasal-temporal ends being the most anterior, and inferior-superior ends being the most posterior. The enface views on the left side of the figure show the points anterior (green) and posterior (red) to the reference planes. The enface images also demonstrate the long ends of the BMO and ALI being more anterior than the short ends. The nonplanarity in ALI was in general greater than in BMO, following a similar pattern but with some rotation in the enface axis angle. Figure 3 shows the BMO and ALI

nonplanarity plotted for all eyes in nonglaucomatous and glaucomatous groups. Between the two groups, BMO nonplanarity was significantly greater in the glaucoma eyes (Table 2) and associated with glaucoma severity (Table 3).

The **distance of the BMO centroid from BM plane** in the posterior direction, which can be contributed by both deformation and displacement of BMO, was negatively associated with axial length in nonglaucomatous eyes and positively associated with glaucoma severity in glaucomatous eyes (Table 3). The distance of the ALI centroid from BM plane was significantly greater in the glaucomatous eyes (Table 2), and positively associated with both axial length and glaucoma severity (Table 3).

Table 4 shows the frequency of **BMO axis direction**, grouped in six sectors with equal angles with reference to superior (S), inferior (I), nasal (N), and temporal (T) orientations. In both groups, BMO axis most frequently lied in the nasal-superior-nasal to nasal sectors. This directionality corresponds with the BMO bowing, and shows that BMO tends to be the most anterior on its longest ends (NSN-TIT to N-T) and most posterior on its shortest ends (IIN-SST to S-I). More BMO axes were in the nasal-temporal sectors for the glaucomatous eyes. BMO axis direction was associated with increased axial length (Table 3), suggesting BMO axis rotation is influenced by both myopia and glaucoma, and BMO nonplanarity and axis rotation may be related in glaucoma.

Table 5 shows the frequency of ALI axis direction. As in BMO, the ALI axis also mainly lied in the nasal-superior-nasal to nasal sectors, corresponding to ALI nonplanarity pattern. There was overall greater variability in the ALI axis of glaucomatous eyes and larger mean axis angle (Table 2).

### Prelaminar Neural Canal

In the nonglaucomatous eyes, prelaminar neural canal (PNC) was longer and more skewed with longer axial length. In the glaucomatous eyes, longer axial length was associated with more skewed canal, and greater glaucoma severity was associated with longer canal, likely due to the posterior cupping and displacement of ALI. Glaucoma severity was also associated with decrease in the BMO-ALIP axis angle difference (Table 3), possibly reflecting the apparent glaucomatous rotation of BMO axis angle toward nasal-temporal axis (Table 4). Table 6 shows the frequency of BMO-to-ALI direction.

### Anterior Laminar Surface

Anterior laminar surface (ALCS) was significantly deeper in the glaucomatous eyes (Table 2) and ALCS depth positively correlated with glaucoma severity (Table 3). However, in both nonglaucomatous and glaucomatous eyes, axial length was negatively correlated with ALCS depth. In nonglaucomatous eyes, longer axial length was significantly associated with less ALCS curvature of the fitted surface.

Table 7 shows the frequency of the location of the ALCS surface minimum. In both groups, ALCS minimum was mainly located in the superior, superior-nasal, and nasal sectors, corresponding to the directions of BMO and ALI elongation and the prelaminar neural canal.

## Discussion

Development of myopia typically begins between age six and fourteen, and the progression stops or slows at the end of adolescence as the general physical growth

ends.[27,28] The axial elongation of the eye during this process affects the structure of the optic nerve head (ONH). On the other hand, most common adult glaucoma occurs in mid-to-late adulthood, with intraocular pressure (IOP)-related deformation and remodeling of the ONH playing a key role in the pathophysiology. Myopia has been associated with increased susceptibility to glaucoma in several population studies,[21–23] and the relationship between myopia and glaucoma involves the myopic ONH structure, the response of the myopic ONH to aging and IOP elevation, and how these affect the onset and progression of glaucoma.

**Literature on myopia and optic nerve head**

- **Optic disk** Early histological studies found that optic disks were **larger** and **more oval** in highly myopic eyes.[29,30] Recent *in vivo* studies showed increasing axial length was associated with **oblique or skewed insertion of the optic nerve into the globe**[31] in fundus photography [32,33] and in 3D optical coherence tomography (OCT) [17,34,35]. The resulting rotation of the major axis of the optic disk in the enface plane (**optic disk torsion**) has been associated with **location of visual field defects** in glaucoma patients[33,36]. A caveat is that the usage of the terms such as optic disk *tilt*, *ovality*, *torsion*, and *skew* have varied across the literature, especially between studies based on 2D fundus photographs and those based on 3D OCT, and the correlation between the 2D and 3D measurements for the supposedly same anatomical measurements has been shown to be limited.[35,37]
- **Lamina cribrosa and sclera** Lamina cribrosa (LC) was found to be significantly **thinner in highly myopic eyes** than in non-highly myopic eyes in both glaucoma

and control groups, resulting in a shorter distance between the intraocular space and cerebrospinal fluid space and increased translaminar pressure gradient.[12] The same experiment also showed that among highly myopic eyes, **presence of glaucoma was associated with thinner LC** than in non-highly myopic eyes. Biomedical models of the sclera further associated myopia with **scleral thinning,**[38,39] **tissue loss,**[39] **failure at a lower load,**[38] **and increase in small diameter collagen fibrils.**[39]

**Literature on myopia and glaucoma**

- Among glaucoma patients, high myopia was identified as a significant risk factor for subsequent **visual field loss**,[40,41] and in examination of glaucomatous optic nerve fiber loss using color stereo optic disc photographs, **optic nerve damage** was shown to be more significant in highly myopic eyes than in non-highly myopic eyes.[42]
- **RNFL thickness** OCT-based measurement of peripapillary retinal nerve fiber layer (RNFL) thickness, a key measurement of glaucoma severity, was also shown to be thinner in healthy myopic subjects.[19,43,44] However, because of the myopic expansion of the optic disk and Bruch's membrane opening, RNFL thickness measurements based on the distance from the centre of the optic disk may be located closer to the BMO for myopic subjects than non-myopic subjects.

**Our study**

**Summary** In this paper, we presented a comprehensive 3D shape characterization and analysis of the anterior laminar region in myopic eyes with and without glaucoma using

images from a custom swept-source optical coherence tomography (SS-OCT) system with a 1060-nm light source. Bruch's membrane opening (BMO), anterior laminar insertion (ALI), prelaminar neural canal (PNC), and anterior lamina cribrosa surface (ALCS) were segmented from the images and analyzed for their relationships with age, axial length, and glaucoma severity. The age-adjusted results showed that the glaucomatous eyes had more bowed and nasally rotated BMO and ALI, more horizontally skewed PNC, and deeper ALCS than the nonglaucomatous eyes. General linear model analysis showed that increased axial length was a significant factor across the anterior laminar region, most notably with a wider, longer, and more horizontally skewed neural canal, and decrease in the ALCS depth and curvature. Such 3D evaluation of the ONH enhances the understanding of the peri-laminar structures and anatomy and can be a complementary tool to the conventional methods of assessment of glaucomatous or suspected glaucomatous eyes.

Serial SD-OCT scans in experimental glaucoma showed that changes in the deeper structures such as the laminar and prelaminar tissues precede other obvious glaucomatous changes such as thinning of the RNFL.[45] The age-adjusted results showed that the glaucomatous eyes had more bowed and nasally rotated BMO and ALI, more horizontally skewed PNC, and deeper ALCS than the nonglaucomatous eyes, which may be a result of the increased intraocular pressure. On the anatomical parameterization, the authors noted that the neural canal opening plane was a valid reference point for assessing and quantifying the ONH parameters, and although the whole neural canal along with the LC may shift posteriorly due to glaucoma, the centroid of the neural canal opening remains stable. Sigler et al.[46] found that prelaminar canal

depth, when measured from the BMO to ALCS, was positively correlated with peripapillary choroidal thickness and this should be considered in modeling. Our study did not explicitly look at the extent of contribution of the peripapillary choroidal thickness to the neural canal length of depth. However, studies have demonstrated choroidal thinning in myopia[47] and this would mean that the neural canal lengthening we observed in the myopic eyes were in spite of any associated choroidal thinning. We also note that our ALCS depth and curvature were defined using only the anterior laminar insertion points and anterior lamina cribrosa surface, without referencing Bruch's membrane or BMO, in order to more accurately capture the shape of the ALCS.

**Myopia & glaucoma's effects in the ONH structure - Compare & Contrast** Our study showed that myopia and glaucoma both affect the ONH structure; however, we note that their underlying mechanisms are fundamentally different. In myopia, the enlarged BMO and ALI areas suggests that the myopic axial elongation of the eye expands the optic neural canal, with the force acting mainly along the scleral wall. In glaucoma, the intraocular pressure acting on the ONH has some laminar component but compared to the myopic expansion it acts more in the axial direction. This simplified model can be useful for interpreting the current result of the ALCS depth being negatively associated with axial length but positively associated with glaucoma severity. In myopia, the enlarging of the canal pulls the LC taut, decreasing its curvature. This model is in line with previous studies in which myopic LC and sclera were shown to be thinner than in nonmyopic eyes.[12,38,39] In glaucoma, the biomechanical model includes posterior bowing or "caving in" of the LC, and in our study the glaucomatous eyes

indeed had deeper ALCS. Increased visual field deviation was also associated with deeper ALCS.

Another parameter affected by both myopia and glaucoma was the enface angle of the BMO and ALI axes, which were more horizontal (closer to temporal-nasal axis) with both greater axial length and glaucoma severity. A myopic mechanism of the phenomenon may be that the myopic expansion of the prelaminar region and in extension scleral opening occurs at a greater degree in the temporal-nasal direction than the superior-inferior direction. A glaucomatous mechanism of the same phenomenon may be that the intraocular pressure affects LC with regional variation.

**So why are myopes more susceptible to glaucomatous damage?** An implication of our study is that the posterior bowing of the LC as a structural parameter of glaucoma severity can be significantly confounded by myopia, and that the myopic LC that is pulled taut, shallower, and thinner than non-myopic eyes may be more vulnerable to mechanical failure and axonal damage inside the LC, despite the reduced global curvature. Previously, in an idealized, analytical microstructural model of the ONH, scleral canal eccentricity, LC stiffness, LC thickness, and eye radius were found to be important determinants of the stress and strain in the LC[48]. Sawada et al. reported that an increased neural canal angle, which correlated with a longer axial length in our study and a recent study by Jeoung et al.[49], was associated with a higher number of temporal LC defects, which in turn spatially corresponded with visual field defects in open-angle glaucoma patients with myopia[50]. The authors posited that the myopic elongation of the globe may lead to stretching of the LC in the temporal periphery, causing localized strain in the LC pores that may become torn and become larger pores that are

susceptible to glaucomatous strain. Such myopic stretching in the temporal direction can also explain the BMO elongation direction we observed in the current study, in which longer axial length was associated with more elongated BMO and more nasal-temporally (horizontally) oriented BMO enface axis.

Age has been reported as a factor in LC deformation. In glaucomatous eyes with the same functional loss, older eyes presented shallower LC[51] and less LC deformation[50] than in younger eyes. This is likely related to the age-related decrease in the mechanical compliance of LC[52]. In our study, age was not a significant factor in the shape parameters in either the nonglaucomatous or glaucomatous groups. This may be attributed to the limited sample size and age distribution, and the effects of myopia and glaucoma being larger than that of age. However, myopic stretching of LC can result in reduction of LC compliance, similarly with aging. Considering that aging and high myopia are two key risk factors in glaucoma, we may conjecture that independent of the degree of glaucomatous global LC deformation (cupping), reduced LC compliance itself, either from aging and/or myopic stretching, may be an important causal factor in the IOP-related axonal damage in glaucoma.

This can further relate to the connection between myopia and normal-tension or low-pressure glaucoma. Studies have demonstrated that the association between myopia and glaucoma were stronger at lower IOP levels than higher IOP levels,[53] and Sigler et al.[46] observed wider horizontal neural canal opening in the low pressure glaucoma group compared to the normal or primary open-angle glaucoma groups. In our study, similar horizontal torsion (T-N axis) and directed expansion of BMO and ALI were observed with increased axial length. These findings suggest that myopia causes

characteristic structural deformation in the optic neural canal region, and this may create a risk factor especially for a certain subtype of glaucoma related to the deformation and lower IOP range.

Funding / Support: Canadian Institutes of Health Research (CIHR), Natural Sciences and Engineering Research Council (NSERC), Michael Smith Foundation for Health Research (MSFHR), Compute Canada, Precision Imaging Beacon – University of Nottingham

Financial disclosures: S. L.: None; M. L.: None; D. R: None; V. R.: None; P. J. M: None; M. V. S.: None; M. F. B.: None

## References

1. Quigley HA, Addicks EM, Green WR, Maumenee AE. Optic nerve damage in human glaucoma. II. The site of injury and susceptibility to damage. *Arch Ophthalmol*. 1981;99(4):635-649. Accessed February 18, 2015. http://www.ncbi.nlm.nih.gov/pubmed/6164357

2. Quigley HA, Hohman RM, Addicks EM, Massof RW, Green WR. Morphologic changes in the lamina cribrosa correlated with neural loss in open-angle glaucoma. *Am J Ophthalmol*. 1983;95(5):673-691. Accessed February 18, 2015. http://www.ncbi.nlm.nih.gov/pubmed/6846459

3. Kwun Y, Han JC, Kee C. Comparison of Lamina Cribrosa Thickness in Normal Tension Glaucoma Patients With Unilateral Visual Field Defect. *Am J Ophthalmol*. 2015;159(3):512-518.e1. doi:10.1016/J.AJO.2014.11.034

4. Roberts MD, Grau V, Grimm J, et al. Remodeling of the connective tissue microarchitecture of the lamina cribrosa in early experimental glaucoma. *Invest Ophthalmol Vis Sci*. 2009;50(2):681-690. doi:10.1167/iovs.08-1792

5. Burgoyne CF. A biomechanical paradigm for axonal insult within the optic nerve head in aging and glaucoma. *Exp Eye Res*. 2011;93(2):120-132. doi:10.1016/j.exer.2010.09.005

6. Yang H, Reynaud J, Lockwood H, et al. The connective tissue phenotype of glaucomatous cupping in the monkey eye - Clinical and research implications. *Prog Retin Eye Res*. 2017;59:1-52. doi:10.1016/j.preteyeres.2017.03.001

7. Bellezza AJ, Rintalan CJ, Thompson HW, Downs JC, Hart RT, Burgoyne CF. Deformation of the lamina cribrosa and anterior scleral canal wall in early experimental glaucoma. *Invest Ophthalmol Vis Sci*. 2003;44(2):623-637. Accessed February 18, 2015. http://www.ncbi.nlm.nih.gov/pubmed/12556392

8. Downs JC, Yang H, Girkin C, et al. Three-dimensional histomorphometry of the normal and early glaucomatous monkey optic nerve head: neural canal and subarachnoid space architecture. *Invest Ophthalmol Vis Sci*. 2007;48(7):3195-3208. doi:10.1167/iovs.07-0021

9. Roberts MD, Sigal IA, Liang Y, Burgoyne CF, Downs JC. Changes in the biomechanical response of the optic nerve head in early experimental glaucoma. *Invest Ophthalmol Vis Sci*. 2010;51(11):5675-5684. doi:10.1167/iovs.10-5411

10. Crawford Downs J, Roberts MD, Sigal IA. Glaucomatous cupping of the lamina cribrosa: a review of the evidence for active progressive remodeling as a mechanism. *Exp Eye Res*. 2011;93(2):133-140. doi:10.1016/j.exer.2010.08.004

11. Grytz R, Sigal IA, Ruberti JW, Meschke G, Downs JC. Lamina Cribrosa Thickening in Early Glaucoma Predicted by a Microstructure Motivated Growth and Remodeling Approach. *Mech Mater*. 2012;44:99-109. doi:10.1016/j.mechmat.2011.07.004

12. Jonas JB, Berenshtein E, Holbach L. Lamina cribrosa thickness and spatial relationships between intraocular space and cerebrospinal fluid space in highly myopic eyes. *Invest Ophthalmol Vis Sci*. 2004;45(8):2660-2665. doi:10.1167/iovs.03-1363

13. Jonas JB, Gusek GC, Naumann GO. Optic disk morphometry in high myopia. *Graefes Arch Clin Exp Ophthalmol*. 1988;226(6):587-590. Accessed February 19, 2015. http://www.ncbi.nlm.nih.gov/pubmed/3209086

14. Jonas JB, Jonas SB, Jonas RA, Holbach L, Panda-Jonas S. Histology of the parapapillary region in high myopia. *Am J Ophthalmol*. 2011;152(6):1021-1029. doi:10.1016/j.ajo.2011.05.006

15. Leung CK-S, Cheng ACK, Chong KKL, et al. Optic disc measurements in myopia with optical coherence tomography and confocal scanning laser ophthalmoscopy. *Invest Ophthalmol Vis Sci*. 2007;48(7):3178-3183. doi:10.1167/iovs.06-1315

16. Hyung SM, Kim DM, Hong C, Youn DH. Optic disc of the myopic eye: relationship between refractive errors and morphometric characteristics. *Korean J Ophthalmol*. 1992;6(1):32-35. Accessed February 19, 2015. http://www.ncbi.nlm.nih.gov/pubmed/1434043

17. Kim M, Choung H-K, Lee KM, Oh S, Kim SH. Longitudinal Changes of Optic Nerve Head and Peripapillary Structure during Childhood Myopia Progression on OCT: Boramae Myopia Cohort Study Report 1. *Ophthalmology*. Published online March 14, 2018. doi:10.1016/J.OPHTHA.2018.01.026

18. Jonas JB, Dichtl A. Optic disc morphology in myopic primary open-angle glaucoma. *Graefes Arch Clin Exp Ophthalmol*. 1997;235(10):627-633. Accessed February 18, 2015. http://www.ncbi.nlm.nih.gov/pubmed/9349946

19. Leung CK-S, Mohamed S, Leung KS, et al. Retinal nerve fiber layer measurements in myopia: An optical coherence tomography study. *Invest Ophthalmol Vis Sci*. 2006;47(12):5171-5176. doi:10.1167/iovs.06-0545

20. Kim MJ, Lee EJ, Kim T-W. Peripapillary retinal nerve fibre layer thickness profile in subjects with myopia measured using the Stratus optical coherence tomography. *Br J Ophthalmol*. 2010;94(1):115-120. doi:10.1136/bjo.2009.162206

21. Mitchell P, Hourihan F, Sandbach J, Wang JJ. The relationship between glaucoma and myopia: the Blue Mountains Eye Study. *Ophthalmology*. 1999;106(10):2010-2015. Accessed February 15, 2015. http://www.ncbi.nlm.nih.gov/pubmed/10519600

22. Xu L, Wang Y, Wang S, Wang Y, Jonas JB. High myopia and glaucoma susceptibility the Beijing Eye Study. *Ophthalmology*. 2007;114(2):216-220. doi:10.1016/j.ophtha.2006.06.050

23. Marcus MW, de Vries MM, Junoy Montolio FG, Jansonius NM. Myopia as a risk factor for open-angle glaucoma: a systematic review and meta-analysis. *Ophthalmology*. 2011;118(10):1989-1994.e2. doi:10.1016/j.ophtha.2011.03.012

24. Young M, Lee S, Rateb M, Beg MF, Sarunic M V, Mackenzie PJ. Comparison of the clinical disc margin seen in stereo disc photographs with neural canal opening seen in optical coherence tomography images. *J Glaucoma*. 2014;23(6):360-367. doi:10.1097/IJG.0b013e31829484a4

25. Lee S, Han SX, Young M, Beg MF, Sarunic M V, Mackenzie PJ. Optic Nerve Head and Peripapillary Morphometrics in Myopic Glaucoma. *Invest Ophthalmol Vis Sci*. 2014;55(7):4378-4393.

26. Bhalla M, Heisler M, Han SX, et al. Longitudinal Analysis of Bruch's Membrane Opening Morphometry in Myopic Glaucoma. *J Glaucoma*. Published online July 19, 2019. doi:10.1097/IJG.0000000000001332

27. Grosvenor T. A review and a suggested classification system for myopia on the basis of age-related prevalence and age of onset. *Am J Optom Physiol Opt*. 1987;64(7):545-554. Accessed June 7, 2018. http://www.ncbi.nlm.nih.gov/pubmed/3307441

28. GONZÁLEZ BLANCO F, SANZ FERŃANDEZ JC, MUŃOZ SANZ MA. Axial Length, Corneal Radius, and Age of Myopia Onset. *Optom Vis Sci*. 2008;85(2):89-96. doi:10.1097/OPX.0b013e3181622602

29. Jonas JB, Gusek GC, Naumann GOH. Optic disk morphometry in high myopia. *Graefe's Arch Clin Exp Ophthalmol*. 1988;226(6):587-590. doi:10.1007/BF02169209

30. Jonas JB. Optic disk size correlated with refractive error. *Am J Ophthalmol*. 2005;139(2):346-348. doi:10.1016/j.ajo.2004.07.047

31. Witmer MT, Margo CE, Drucker M. Tilted Optic Disks. *Surv Ophthalmol*. 2010;55(5):403-428. doi:10.1016/j.survophthal.2010.01.002

32. Tay E, Seah SK, Chan S-P, et al. Optic disk ovality as an index of tilt and its relationship to myopia and perimetry. *Am J Ophthalmol*. 2005;139(2):247-252. doi:10.1016/J.AJO.2004.08.076

33. Choi JA, Park H-YL, Shin H-Y, Park CK. Optic Disc Tilt Direction Determines the Location of Initial Glaucomatous Damage. *Investig Opthalmology Vis Sci*. 2014;55(8):4991. doi:10.1167/iovs.14-14663

34. Marsh-Tootle WL, Harb E, Hou W, et al. Optic Nerve Tilt, Crescent, Ovality, and Torsion in a Multi-Ethnic Cohort of Young Adults With and Without Myopia. *Investig Opthalmology Vis Sci*. 2017;58(7):3158. doi:10.1167/iovs.16-20860

35. Hosseini H, Nassiri N, Azarbod P, et al. Measurement of the Optic Disc Vertical Tilt Angle With Spectral-Domain Optical Coherence Tomography and Influencing Factors. *Am J Ophthalmol*. 2013;156(4):737-744.e1. doi:10.1016/j.ajo.2013.05.036

36. Park H-YL, Lee K, Park CK. Optic Disc Torsion Direction Predicts the Location of Glaucomatous Damage in Normal-Tension Glaucoma Patients with Myopia. *Ophthalmology*. 2012;119(9):1844-1851. doi:10.1016/J.OPHTHA.2012.03.006

37. Takasaki H, Higashide T, Takeda H, Ohkubo S, Sugiyama K. Relationship between optic disc ovality and horizontal disc tilt in normal young subjects. *Jpn J Ophthalmol*. 2013;57(1):34-40. doi:10.1007/s10384-012-0193-9

38. Phillips JR, McBrien NA. Form deprivation myopia: elastic properties of sclera. *Ophthalmic Physiol Opt*. 1995;15(5):357-362. Accessed July 16, 2018. http://www.ncbi.nlm.nih.gov/pubmed/8524554

39. McBrien NA, Cornell LM, Gentle A. Structural and ultrastructural changes to the sclera in a mammalian model of high myopia. *Invest Ophthalmol Vis Sci*. 2001;42(10):2179-2187. Accessed July 16, 2018. http://www.ncbi.nlm.nih.gov/pubmed/11527928

40. Chihara E, NIL X, Dong J, et al. Severe Myopia as a Risk Factor for Progressive Visual Field Loss in Primary Open-Angle Glaucoma. *Ophthalmologica*. 1997;211(2):66-71. doi:10.1159/000310760

41. Han JC, Lee EJ, Kim SH, Kee C. Visual Field Progression Pattern Associated With Optic Disc Tilt Morphology in Myopic Open-Angle Glaucoma. *Am J Ophthalmol*. 2016;169:33-45. doi:10.1016/J.AJO.2016.06.005

42. Jonas JB, Budde WM. Optic nerve damage in highly myopic eyes with chronic open-angle glaucoma. *Eur J Ophthalmol*. 2005;15(1):41-47. Accessed February 18, 2015. http://www.ncbi.nlm.nih.gov/pubmed/15751238

43. Rauscher FM, Sekhon N, Feuer WJ, Budenz DL. Myopia affects retinal nerve fiber layer measurements as determined by optical coherence tomography. *J Glaucoma*. 2009;18(7):501-505. doi:10.1097/IJG.0b013e318193c2be

44. Kang SH, Hong SW, Im SK, Lee SH, Ahn MD. Effect of myopia on the thickness of the retinal nerve fiber layer measured by Cirrus HD optical coherence tomography. *Invest Ophthalmol Vis Sci*. 2010;51(8):4075-4083. doi:10.1167/iovs.09-4737

45. Strouthidis NG, Fortune B, Yang H, Sigal IA, Burgoyne CF. Longitudinal change detected by spectral domain optical coherence tomography in the optic nerve head and peripapillary retina in experimental glaucoma. *Invest Ophthalmol Vis Sci*. 2011;52(3):1206-1219. doi:10.1167/iovs.10-5599

46. Sigler EJ, Mascarenhas KG, Tsai JC, Loewen NA. Clinicopathologic correlation of disc and peripapillary region using SD-OCT. *Optom Vis Sci*. 2013;90(1):84-93. doi:10.1097/OPX.0b013e318278fc15

47. Read SA, Fuss JA, Vincent SJ, Collins MJ, Alonso-Caneiro D. Choroidal changes in human myopia: insights from optical coherence tomography imaging. *Clin Exp Optom*. 2019;102(3):270-285. doi:10.1111/cxo.12862

48. Sander EA, Downs JC, Hart RT, Burgoyne CF, Nauman EA. A cellular solid model of the lamina cribrosa: Mechanical dependence on morphology. *J Biomech Eng*. 2006;128(6):879-889. doi:10.1115/1.2354199

49. Jeoung JW, Yang H, Gardiner S, et al. Optical Coherence Tomography Optic

Nerve Head Morphology in Myopia I: Implications of Anterior Scleral Canal Opening Versus Bruch Membrane Opening Offset. *Am J Ophthalmol*. 2020;218:105-119. doi:10.1016/j.ajo.2020.05.015

50. Sawada Y, Araie M, Ishikawa M, Yoshitomi T. Multiple Temporal Lamina Cribrosa Defects in Myopic Eyes with Glaucoma and Their Association with Visual Field Defects. *Ophthalmology*. 2017;124(11):1600-1611. doi:10.1016/j.ophtha.2017.04.027

51. Ren R, Yang H, Gardiner SK, et al. Anterior lamina cribrosa surface depth, age, and visual field sensitivity in the Portland progression project. *Investig Ophthalmol Vis Sci*. 2014;55(3):1531-1539. doi:10.1167/iovs.13-13382

52. Albon J, Purslow PP, Karwatowski WSS, Easty DL. Age related compliance of the lamina cribrosa in human eyes. *Br J Ophthalmol*. 2000;84(3):318-323. doi:10.1136/bjo.84.3.318

53. Grødum K, Heijl A, Bengtsson BB. Refractive error and glaucoma. *Acta Ophthalmol Scand*. 2001;79(6):560-566. doi:10.1034/j.1600-0420.2001.790603.x

# Tables

*Table 1. **Participant summary** Number of Subjects, Number of Eyes, and mean ± SD (minimum – maximum) Age, Axial Length, and visual field index (Mean Deviation) of nonglaucomatous and glaucomatous participants*

| | Nonglaucomatous | Glaucomatous | P |
|---|---|---|---|
| **Number of Subjects** | 19 (10 females) | 38 (15 females) | |
| **Number of Eyes** | 38 | 63 | |
| **Age** | 37.3 ± 13.9 (20-61) | 61.2 ± 12.5 (30-84) | <.001 |
| **Axial Length (mm)** | 25.1 ± 1.42 (23.1 – 28.42) | 25.9 ± 1.78 (22.5-31.28) | - |
| **Mean Deviation (dB)** | -0.91 ± 1.00 (-.06 – 0.97) | -11.9 ± 8.82 (-33.6 – 0.83) | <.001 |

*Table 2. Mean measurements of Bruch's membrane opening (BMO), anterior laminar insertion point (ALI) ellipse, prelaminar neural canal (PNC) and anterior laminar surface (ALCS) for healthy and glaucomatous eyes. An asterisk indicates p < .001.*

| | Nonglaucomatous | Glaucomatous | P |
|---|---|---|---|
| **BMO** | | | |
| **Area ($mm^2$)** | 2.29 ± 0.83 | 2.26 ± 0.62 | - |
| **Eccentricity** | 1.13 ± 0.09 | 1.14 ± 0.07 | - |
| **Nonplanarity (µm)** | 8.18 ± 3.51 | 9.67 ± 3.73 | .026 |
| **Centroid distance from BM (mm)** | 0.116 ± 0.055 | 0.137 ± 0.042 | - |
| **Axis angle (°)** | 64.7 ± 20.2 | 77.9 ± 20.3 | - |
| **ALI** | | | |
| **Area ($mm^2$)** | 2.97 ± 0.83 | 2.86 ± 0.67 | - |
| **Eccentricity** | 1.13 ± 0.05 | 1.15 ± 0.08 | .037 |
| **Nonplanarity (µm)** | 25.5 ± 7.56 | 28.7 ± 10.1 | - |
| **Centroid distance from BM (mm)** | 0.395 ± 0.059 | 0.447 ± 0.132 | - |
| **Axis angle (°)** | 66.4 ± 24.2 | 87.1 ± 47.1 | .029 |
| **PNC** | | | |
| **Canal height (mm)** | 0.247 ± 0.061 | 0.194 ± 0.059 | - |
| **Canal width (mm)** | 0.275 ± 0.186 | 0.391 ± 0.246 | - |
| **Canal length (mm)** | 0.394 ± 0.175 | 0.480 ± 0.224 | - |
| **Canal angle (°)** | 43.2 ± 18.9 | 54.4 ± 21.0 | - |
| **BMO-ALI angle (°)** | 74.5 ± 27.4 | 73.4 ± 14.6 | - |
| **ALCS** | | | |
| **ALCS depth (mm, seg points)** | 0.109 ± 0.046 | 0.143 ± 0.048 | <.001* |
| **Relative ALCS depth ($mm^{-1}$, seg points)** | 0.040 ± 0.023 | 0.050 ± 0.019 | .003 |
| **ALCS depth (mm) (fitted surface)** | 0.096 ± 0.043 | 0.131 ± 0.050 | <.001* |
| **ALCS mean principal curvature ($mm^{-1}$)** | 0.325 ± 0.164 | 0.381 ± 0.112 | .001 |
| **ALCS minimum - ALI centroid Dist. (%)** | 6.51 ± 3.68 | 7.10 ± 3.30 | - |

*Table 3. Significant p-values from general linear models of Bruch's membrane opening (BMO), anterior laminar insertion (ALI), prelaminar neural canal (PNC), and anterior laminar surface (ALCS) measurements with age, axial length (AL), and visual field index (MD) as predictors of nonglaucomatous and glaucomatous eyes. Red indicates the predictor was negatively associated with the variable.*

| | Nonglaucomatous | | Glaucomatous | | |
|---|---|---|---|---|---|
| | Age | AL | Age | AL | MD |
| **BMO** | | | | | |
| **Area ($mm^2$)** | - | .008* | - | .003* | - |
| **Eccentricity** | - | .010 | - | .018 | - |
| **Nonplanarity (µm)** | - | - | - | - | .039 |
| **Centroid distance from BM (mm)** | - | .018 | - | - | .004 |
| **Axis angle (°)** | - | .009* | - | - | - |
| **ALI** | | | | | |
| **Area ($mm^2$)** | - | .014 | - | .011 | - |
| **Eccentricity** | - | - | - | - | - |
| **Nonplanarity (µm)** | - | - | - | - | - |
| **Centroid distance from BM (mm)** | - | - | - | .030 | <.001* |
| **Axis angle (°)** | - | - | - | - | - |
| **PNC** | | | | | |
| **Canal height (mm)** | - | .004* | - | - | - |
| **Canal width (mm)** | - | <.001* | - | .025 | - |
| **Canal length (mm)** | - | <.001* | - | - | .025 |
| **Canal angle (°)** | - | <.001* | - | - | - |
| **BMO-ALI angle (°)** | - | - | - | - | .036 |
| **ALCS** | | | | | |
| **ALCS depth (mm, points)** | - | .037 | - | - | .002* |
| **Relative ALCS depth ($mm^{-1}$, points)** | - | .011 | - | .005* | <.001* |
| **ALCS depth (mm) (fitted surface)** | - | .047 | - | - | - |
| **ALCS mean principal curvature ($mm^{-1}$)** | - | .002* | - | - | - |
| **ALCS minimum - ALI centroid Dist. (%)** | - | - | - | - | - |

Table 4. Frequency of Bruch's membrane opening (BMO) axis directions

| | S-I | SSN-IIT | NSN-TIT | N-T | NIN-STS | IIN-SST |
|---|---|---|---|---|---|---|
| **Nonglaucomatous (n = 38)** | 2 | 8 | 16 | 10 | 1 | 1 |
| **Glaucomatous (n = 63)** | 2 | 8 | 18 | 26 | 6 | 3 |

Table 5. Frequency of anterior laminar insertion (ALI) axis directions

| | S-I | SSN-IIT | NSN-TIT | N-T | NIN-STS | IIN-SST |
|---|---|---|---|---|---|---|
| **Nonglaucomatous (n = 38)** | 2 | 4 | 18 | 12 | 1 | 1 |
| **Glaucomatous (n = 63)** | 9 | 8 | 13 | 18 | 7 | 9 |

Table 6. Frequency of BMO to ALI direction

| | S | SN | N | IN | I | IT | T | ST |
|---|---|---|---|---|---|---|---|---|
| **Nonglaucomatous (n = 38)** | 1 | 11 | 18 | 1 | 0 | 3 | 1 | 3 |
| **Glaucomatous (n = 63)** | 3 | 18 | 34 | 1 | 1 | 2 | 0 | 4 |

Table 7. Frequency of anterior laminar surface minimum location

| | S | SN | N | IN | I | IT | T | ST |
|---|---|---|---|---|---|---|---|---|
| **Nonglaucomatous (n = 38)** | 7 | 15 | 7 | 1 | 2 | 3 | 4 | 2 |
| **Glaucomatous (n = 63)** | 17 | 27 | 8 | 0 | 2 | 0 | 4 | 8 |

## Figure Legends

*Figure 1.* ***Optic nerve head shape parameterization****. A) Bruch's membrane (red curve), Bruch's membrane opening (BMO, red dot), prelaminar neural canal (yellow curve), anterior laminar insertion points (ALIP, blue dots), and anterior lamina cribrosa surface (ALCS, pink dot). B) BMO and ALIP centroids (white dot) and major and minor axes (white dotted line). C) PNC height (h), width (w), length (l), and angle (θ). D) ALCS depth (magenta arrows), ALIP centroid (white dot), ALCS deepest point (white asterisk), and off-centre distance (white line).*

*Figure 2.* ***Bruch's membrane opening (BMO) and anterior laminar insertion (ALI) nonplanarity***

*Figure 3.* ***Bruch's membrane opening points (top) and anterior laminar insertion points (bottom) in reference to the best-fit plane for nonglaucomatous and glaucomatous eyes.***

FIGURG 1

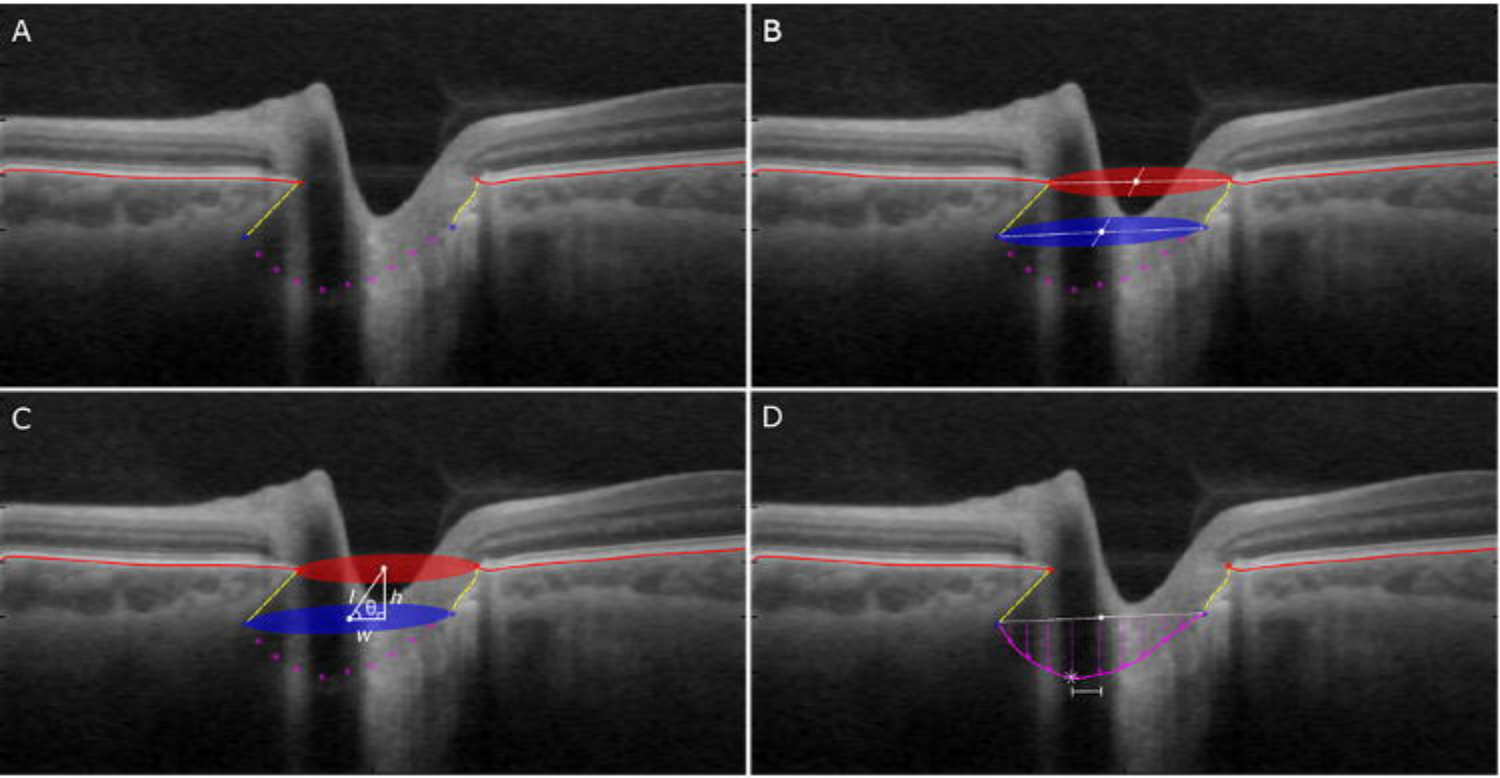

FIGURE 2

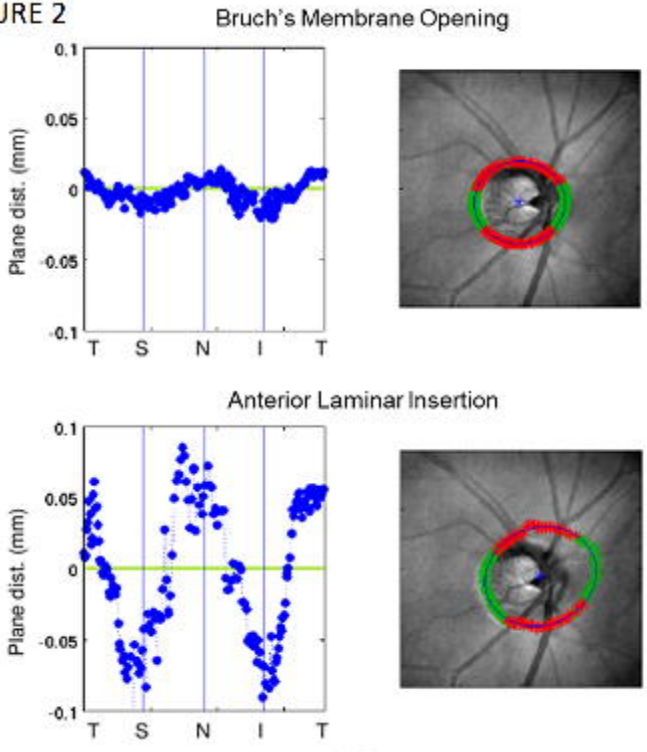
Bruch's Membrane Opening
Plane dist. (mm)
0.1
0.05
0
-0.05
-0.1
T
S
N
I
T
Anterior Laminar Insertion
Plane dist. (mm)
0.1
0.05
0
-0.05
-0.1
T
S
N
I
T

FIGURE 3

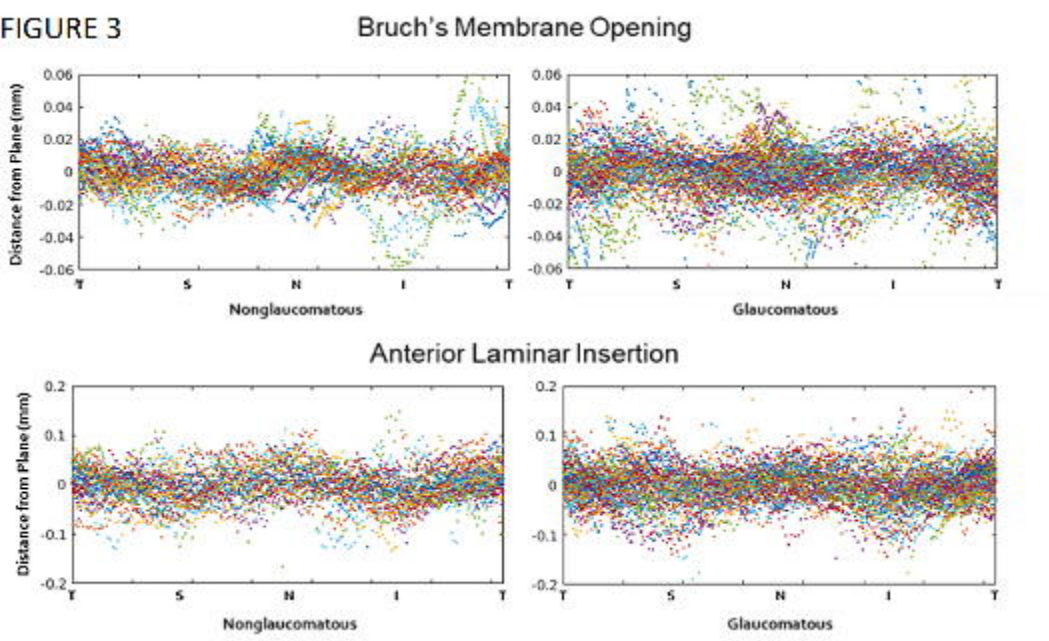
Bruch's Membrane Opening
Distance from Plane (mm)
0.06
0.04
0.02
0
-0.02
-0.04
-0.06
T
S
N
I
T
Nonglaucomatous
Glaucomatous
Anterior Laminar Insertion
0.2
0.1
-0.1
-0.2